# A Multipipe Model of General Strip Transmission Lines for Rapid Convergence of Integral Equation Singularities

Gregory E. Howard, *Member, IEEE*, Jian Jun Yang, *Member, IEEE*, and Y. Leonard Chow, *Member, IEEE*

*Abstract*—**An integral equation for solving thin conducting strip problems always involves three singularities, viz, two charge singularities at the strip edges and the Green's function singularity for close proximity of source and field points. This paper overcomes the singularity convergence problem using Gauss–Chebyshev quadrature for the edge charges, but more importantly by a multipipe model for the Green's function singularity. This model applies equally well to both two-dimensional (2-D) and three-dimensional (3-D) problems of metallic strips embedded in multilayer dielectric substrates. To reduce the scope, however, this paper analyzes only the quasi-TEM cases of 2-D thin strip transmission lines in multilayer dielectric substrates.**

## I. Introduction

THE QUASI-TEM formulation is often used in studying the propagation characteristics of multi-strip transmission lines in multilayer dielectric media [1]–[10]. The formulation assumes as TEM wave along the transmission line and solves an electrostatic field problem in the transverse dimensions. Although solvable by the 2-D finite element method [10], the infinite extent of the static field over the transverse plane causes the problem of multi-strip transmission lines to be solved more frequently by a 2-D integral equation and the method of moments [1]–[9].

The integrand of the integral equation, even for a single strip, involves three singularities, namely, the charge singularity at the two edges of the strip and the Green's function singularity where source and field points coincide. To better describe the high field or charge density near the singularities, fine segmentation in the moment method solution is required. This means that the matrix from the moment method procedure must be quite large and causes slow convergence in the solution. To improve the numerical efficiency, therefore, one must avoid fine segmentation around the singularities.

In this paper, the charge singularities at the strip edges are avoided by using Gauss–Chebyshev quadrature, since this quadrature has the correct singular weighting function to represent the charge density across the strip. The Green's function singularity is avoided by constructing uniform charge pipes centering at the Gauss–Chebyshev quadrature matching points. As a result, the matrix size is reduced by an order of magnitude when compared to the use of pulse basis functions [1], [4].

The multipipe model introduced in this paper is similar to that introduced by Wheeler [13]. Wheeler assumes true conductive pipes with *nonuniform* charge distribution around the pipe due to proximity effects. The nonuniform charge distribution makes the field calculation difficult. This paper assumes nonconductive pipes with bound charges *uniformly* distributed around the pipe perimeters. Because of the uniform charge distribution, the field from each charged pipe is circularly symmetric and is very simple. This difference means that the pipe radii derived in this paper are different from those of Wheeler. This will be observed in Table I.

In the following, the multipipe model is first derived for a thin strip conductor in free space, for which the rigorous conformal mapping solution is known [12]. While the singularity locations do not change, the charge density across the strip changes with the inclusion of multilayer dielectric substrates and the proximity effects of the adjacent strips. It is proved (in Section II-B) that regardless of this change, the above multipipe model with Gauss–Chebyshev quadrature still applies with high accuracy and small matrix size.

## II. The Multipipe Model

### A. The Multipipe Model of a Single Thin Strip in Free Space

Through conformal mapping, Wheeler [13] has shown that the potential $V_0$ on a conductive strip of width $w$, Fig. 1(a), is the same as the potential on a conductive pipe of radius $w/4$. With a known surface charge distribution ($C/m^2$) over the strip:

$$\sigma(x') = \frac{P_0}{\sqrt{1 - (2x'/w)^2}} \tag{1}$$

Manuscript received September 10, 1991; revised December 2, 1991. This work was supported by the National Science and Engineering Research Council of Canada, through operating grant A3804.

G. E. Howard is with the University of British Columbia, Vancouver, BC, Canada.

J. J. Yang and Y. L. Chow are with the Department of Electrical and Computer Engineering, University of Waterloo, Waterloo, ON, Canada N2L 3G1.

IEEE Log Number 9106331.

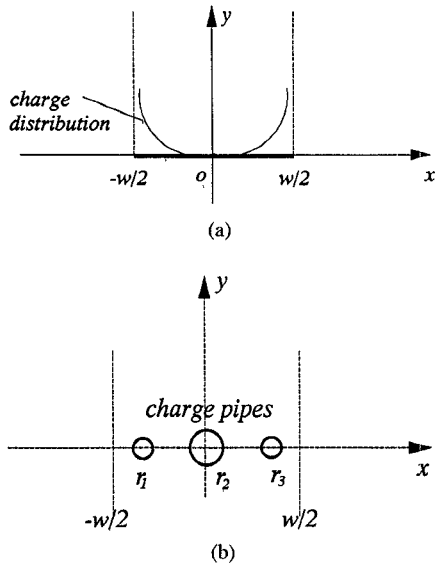


Fig. 1. (a) Strip conductor in free space. (b) Three-pipe model for the strip conductor of Fig. 1(a).

where $P_0$ is a constant, the above statement means that the potential on the strip can be written as

$$V_1(0) = V_0 = \frac{-P_0 w}{4\epsilon_0} \ln (w/4) \tag{2}$$

with a unit radius zero potential reference for the line charge. The subscript "1" is used to distinguish the one-pipe model. One can also write an integral relating the voltage $V(x) = V_0$ on the strip to the surface charge $\sigma(x)$. That is

$$V_0 = V(x)|_{-w/2 < x < w/2} = \int_{-w/2}^{w/2} \sigma(x)\, G_0(x, x')\, dx' \tag{3}$$

where $G_0(x, x')$ is the 2-D Green's function in free space:

$$G_0(x, x') = -\frac{1}{2\pi\epsilon_0} \ln |x - x'|. \tag{4}$$

The integral (3) need not be evaluated since the voltage $V(x) = V_0$ is already known from (2).

If this integral were to be evaluated, say numerically, one would see a problem of three singularities in the integrand, namely, the singularities of $\sigma(x)$ at $|x| = w/2$ and the singularity of the 2-D Green's function when $x = x'$. Such singularities result in slow convergence in the moment method solution, when (3) is used as an integral equation.

If one ignores the Green's function singularity, the problem of the charge singularity of $\sigma(x)$ can easily be eliminated by using an $N$th order Gauss–Chebyshev quadrature in the form

$$V_0 = V_N(x) \approx \frac{\pi w P_0}{2N} \sum_{n=1}^{N} G_0(x_m, x_n'). \tag{5}$$

When the potential is evaluated at the quadrature points $x_m$, the use of Gauss–Chebyshev quadrature results in a logarithmic term which diverges at $x_m = x_n'$:

$$V_0 = V_N(x_m) \approx \frac{\pi w P_0}{2N} \left[ \sum_{\substack{n=1 \\ n \neq m}}^{N} G_0(x_m, x_n') + \left(\frac{-1}{2\pi\epsilon_0}\right) \lim_{x_m \to x_n'} \ln |x_m - x_n'| \right]. \tag{6}$$

The quadrature fails because of the Green's function singularity. From (2) it is known that $V_N(x_m) = V_0$, a finite constant at the quadrature points. Therefore this failure can be corrected by replacing the singular factor in (6) by a constant, $\ln (r_m)$. The value of $r_m$ can be obtained by equating $V_1(0)$ to $V_N(x_m)$ for each quadrature point. With some minor manipulations, one gets

$$\frac{r_m}{(w/4)} = \frac{1}{\sum_{\substack{n=1 \\ n \neq m}}^{N} \left| \frac{x_n - x_m}{(w/4)} \right|}, \qquad N > 1, \quad m = 1, \cdots, N. \tag{7}$$

For $N = 1$, in place of (7), we have

$$r_1 = w/4. \tag{8}$$

Thus (6) is changed to

$$V_0 = V_N(x_m) \approx \sum_{\substack{n=1 \\ n \neq m}}^{N} q_n G_0(x_m, x_n') + q_m G_0(0, r_m) \tag{9}$$

where $q_n = q_m = \pi w P_0/(2N)$. Since $r_m$ at the right-hand side is adjusted in (7) to satisfy (9), the above equation does not diverge, and is exact for the single thin strip in free space. Thus the Green's function singularity of (4) in the integral equation (3) is overcome. This last term of $x_m = x_n'$ may be called the self term.

Equation (9) represents the potentials $V_0$ at matching points $x_m$; each matching point is surrounded by a pipe of radius $r_m$ with a uniform surface charge density $\sigma_m$. Each surface charge $\sigma_m$ integrated over the pipe azimuth angle gives the same line charge of $q_m$ (C/m).

Since the voltages at the pipe centers $x_m$ are $V_0$, the above interpretation means that the conducting strip is replaced by the $N$ pipes of uniform charge density. The replacement is exact for the potentials at the centers $x_m$ of the pipes. A 3-pipe replacement of the thin strip in Fig. 1(a) is illustrated in Fig. 1(b). It is noted that the total charge of the $N$ pipes equals to the total charge over the strip.

Given below is Table I tabulating different pipe radii for different pipe orders (number of pipes) calculated from (7). It may be noted that the multipipe method here gives different radii in Table I compared to those given by Wheeler [13]. The difference lies on the fact that Wheeler chooses conductive pipes, but this paper chooses charge pipes of *uniform* density. Because of our choice, the pipe radii in (7) and the potential field in (9) become very simple.

TABLE I
NORMALIZED PIPE RADII $r_m/(w/4)$ FOR VARIOUS PIPE ORDER $N$

| | Pipe Index $m$ | | | | |
|---|---|---|---|---|---|
| Pipe Order $N$ | 1 | 2 | 3 | 4 | 5 |
| 1 | 1.00 | | | | |
| 2 | 0.3536 | 0.3536 | | | |
| 3 | 0.1667 | 0.3333 | 0.1667 | | |
| 4 | 0.0956 | 0.2310 | 0.2310 | 0.0957 | |
| 5 | 0.0618 | 0.1618 | 0.2000 | 0.1618 | 0.0618 |

The pipe radii decrease towards the edge since the charge density increases towards the edge. This is a direct result of the voltage matching condition applied in (9).

From the derivation process of the multipipe model, it should also be noticed that the pipe radii are solely determined by the strip width $w$ and the number of pipes $N$. The pipe radii do not change for a conducting strip in different coupling situations. It is the pipe weighting coefficients, like $q_n$ in (9), that will be adjusted using the moment method to take into account all the mutual coupling. The moment method using the multipipe model will be described in the next subsection.

### *B. The Multipipe Model for a Thin Strip in a Layered Dielectric*

This section proves that the multipipe model for a strip in free space can still be used for a general strip embedded in a layered dielectric with or without ground planes.

Similar to (3), the voltage $V(x) = V_0$ on the strip in a layered dielectric and the surface charge density $\sigma(x)$ are related through the following integral:

$$V_0 = V(x)|_{-w/2<x<w/2} = \int_{-w/2}^{w/2} \sigma(x')\, G(x, x')\, dx' \tag{10}$$

where the charge distribution of $\sigma(x')$ on the strip is different from (1) in free space due to the presence of layered dielectric. It is generally represented as follows:

$$\sigma(x') = \frac{P(x')}{\sqrt{1 - (2x'/w)^2}} \tag{11}$$

where $P(x')$ is an unknown factor in the charge density on the strip and was equal to a constant $P_0$ for an isolated strip in free space. The Green's function $G(x, x')$ is also different from the free space Green's function (4). Using the image technique (real images for a homogeneous medium with a ground plane, or complex images for a multilayer dielectric medium [11]; real images may be considered as a special case of complex images), the Green's function can be generally written in the following form:

$$G(x, x') = G_{\text{source}}(x, x') + G_{\text{image}}(x, x') \tag{12}$$

where

$$G_{\text{source}} = \frac{-1}{2\pi\epsilon} \ln |x - x'| \tag{13}$$

represents the source term, i.e., the potential of a line charge in a homogeneous medium of permittivity $\epsilon$, and

$$G_{\text{image}} = \frac{-1}{2\pi\epsilon} \sum_{i=1}^{N_{\text{image}}} a_i \ln \sqrt{(x - x')^2 + b_i^2} \tag{14}$$

represents the image terms which take into account all the dielectric layers and ground planes. The images are located in the same homogeneous medium of permittivity $\epsilon$. But they are separated from the original line source by a distance $b_i$ (real or complex) in $y$-dimension. In all the examples tested in this paper, the number of complex images, $N_{\text{image}}$, is taken as 5.

The concept of complex images has been used before in solving dipole and line source radiation problems in a dielectric half space [18]. For the electrostatic field computation in multilayered media, we derived a complex image expression by numerically processing a known spectral function of the layered media [11]. The complex image technique of [11] does not have any limitation on the number of dielectric layers, so long as the spectral function is known. The spectral functions of the dielectric structure shown in Fig. 2, having three optional dielectric layers and two optional ground planes, are tabulated in the Appendix.

Substituting (12) into (10), and evaluating the voltage at the Gauss–Chebyshev quadrature points $x_m$, we can rewrite (10) as follows:

$$\begin{aligned} V_0 = V(x_m) &= \int_{-w/2}^{w/2} \sigma(x')\, G_{\text{source}}(x_m, x')\, dx' \\ &\quad + \int_{-w/2}^{w/2} \sigma(x')\, G_{\text{image}}(x_m, x')\, dx' \\ &= V_{\text{source}}(x_m) + V_{\text{image}}(x_m). \end{aligned} \tag{15}$$

Since the images are always away from the original strip by a distance $b_i \neq 0$, the integrand of the second term in (15) has no Green's function singularity. Thus Gauss–Chebyshev quadrature integration applies directly even when $x' = x_m$, i.e.:

$$V_{\text{image}}(x_m) = \frac{\pi w}{2N} \sum_{n=1}^{N} P(x_n')\, G_{\text{image}}(x_m, x_n'). \tag{16}$$

The integrand of the first term in (15) has a Green's function singularity at $x' = x_m$. To overcome this singularity, the voltage $V_{\text{source}}(x_m)$ is rewritten as follows:

$$\begin{aligned} V_{\text{source}}(x_m) &= \int_{-w/2}^{w/2} \frac{P(x')}{\sqrt{1 - (2x'/w)^2}}\, G_{\text{source}}(x_m, x')\, dx' \\ &= \int_{-w/2}^{w/2} \frac{P(x') - P(x_m)}{\sqrt{1 - (2x'/w)^2}}\, G_{\text{source}}(x_m, x')\, dx' \\ &\quad + P(x_m) \int_{-w/2}^{w/2} \frac{1}{\sqrt{1 - (2x'/w)^2}} \\ &\quad \cdot G_{\text{source}}(x_m, x')\, dx' \\ &= I_1 + I_2. \end{aligned} \tag{17}$$

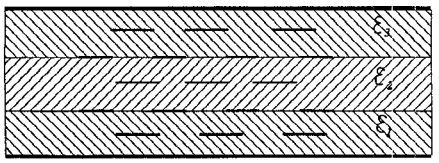


Fig. 2. Multiconductor transmission lines in a multilayer dielectric.

In the integrand of the first integral of (17), the factor $P(x') - P(x_m)$ has a first-order zero at $x' = x_m$. With $G_{\text{source}}$ defined as a logarithmic function in (13), it can be easily shown by L'Hopital's rule that the integrand is reduced to zero at $x' = x_m$. Therefore by the Gauss-Chebyshev quadrature, we have

$$I_1 = \frac{\pi w}{2N} \sum_{\substack{n=1 \\ n \neq m}}^{N} [P(x_n') - P(x_m)]\, G_{\text{source}}(x_m, x_n') - \frac{w}{4\epsilon N} \lim_{x_m \to x_n'} [P(x_n') - P(x_m)] \ln |x_m - x_n'| = \frac{\pi w}{2N} \sum_{\substack{n=1 \\ n \neq m}}^{N} [P(x_n') - P(x_m)]\, G_{\text{source}}(x_m, x_n'). \quad (18)$$

The second integral of (17) still has the Green's function singularity. But it is simply the solution to (3) for the strip in free space, multiplied by the charge distribution $P(x_m)$ at $x_m$. Hence,

$$I_2 = P(x_m) \int_{-w/2}^{w/2} \frac{1}{\sqrt{1 - (2x'/w)^2}}\, G_{\text{source}}(x_m, x')\, dx' = \frac{\pi w}{2N} P(x_m) \left[ \sum_{\substack{n=1 \\ n \neq m}}^{N} G_{\text{source}}(x_m, x_n') + G_{\text{source}}(0, r_m) \right] \quad (19)$$

Adding the two integrals $I_1$ and $I_2$ yields the following simple result for $V_{\text{source}}(x_m)$

$$V_{\text{source}}(x_m) = \frac{\pi w}{2N} \left[ \sum_{\substack{n=1 \\ n \neq m}}^{N} P(x_n')\, G_{\text{source}}(x_m, x_n') + P(x_m)\, G_{\text{source}}(x_m, x_m') \right]. \quad (20)$$

Substituting (16) and (20) into (15), and using the definitions of (13) and (14), the voltage at the quadrature points $x_m$ can be written as follows

$$V_0 = V(x_m) = \sum_{n=1}^{N} q_n G_{mn}, \qquad m = 1, 2, \cdots N \quad (21)$$

where $q_n = \pi w P_1(x_n')/2N$ is the unknown to be solved, and

$$G_{mn} = \begin{cases} G_{\text{source}}(x_m, x_n') + G_{\text{image}}(x_m, x_n'), & m \neq n \\ G_{\text{source}}(0, r_m) + G_{\text{image}}(x_m, x_m'), & m = n. \end{cases} \quad (22)$$

The pipe radii $r_m$ used in (22) are the same as given by (7) and Table I. Obviously, the unknown charge coefficients $q_n$ can be solved from the matrix equation (21).

### *C. The Multipipe Model for Solving the Capacitance Matrix of Multiple Strips*

The above multipipe model can be used for multiple thin strips embedded in a layered dielectric. The first step is to replace each strip by a given number of uniformly charged pipes, $N_i$, where $i$ ranges from 1 to $N_{\text{strips}}$, the number of strips being modeled. The second step is to match the potential on all the strips, at the $N$ pipe-centers on each strip. This yields a matrix equation from which the unknown charge coefficients $q_n$ can be solved.

With the matrix equation solved, the mutual capacitance $C_{ij}$ between the $i$th strip and the $j$th strip can be calculated using the following formula, when the $j$th strip has the potential $V_j$ and the rest of the strips have zero potential:

$$C_{ij} = \frac{\sum_{m=1}^{N_i} q_m}{V_j}, \qquad i, j = 1, 2, \cdots N_{\text{strips}}. \quad (23)$$

It can be easily shown that the above capacitance is variational with respect to the charge distribution.

## Numerical Examples

Based on the multipipe technique and the complex image technique, we have developed a general program for calculating the capacitance and inductance matrices of transmission line structures shown in Fig. 2. Given below are six examples tested, i.e., a single microstrip line, two tightly coupled microstrip lines, two strips between two ground planes, three strips in three dielectric layers between two ground planes, six strips on a dielectric substrate above a ground plane, and a broadside coupled suspended stripline.

### *Example 1: A Single Microstrip Line*

Fig. 3 shows a single microstrip of zero thickness on a dielectric substrate above a ground plane. The characteristic impedance $Z_0$ of the microstrip is $Z_0 = 1/(v_0\sqrt{CC_0})$, where $v_0$ is the speed of light in free space, $C$ is the capacitance of the microstrip and $C_0$ is the free space capacitance of the microstrip. For various $w/h$ ratios, Table II compares our results for $Z_0$ with those of [4], [5]. Our results were obtained by using 3 pipes, i.e., the matrix size is $3 \times 3$, except for the case of $w/h = 10$ where 8 pipes were required for the given accuracy. In [4], the matrix size was $42 \times 42$.

To show the convergence of our results, Fig. 4 plots the percentage difference in the microstrip characteristic impedance $Z_0$ between our results and those of [15], versus the number of pipes $N$. In our calculations, the computer time for the 8-pipe model is less than 6 s on a CSS-386 personal computer. It is seen in Fig. 4 that when the

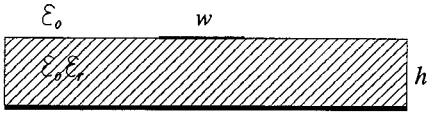


Fig. 3. Single microstrip line.

TABLE II
CHARACTERISTIC IMPEDANCE $Z_0$ IN OHMS FOR A SINGLE MICROSTRIP LINE (FIG. 3)

| | $\epsilon_r = 6.0$ | | | | $\epsilon_r = 9.8$ | | |
|---|---|---|---|---|---|---|---|
| $w/h$ | Our Results | Reference [4] | % Difference from [4] | Reference [5] | Our Results | Reference [15] | % Difference from [15] |
| 0.4 | 90.40 | 92.28 | −2.08 | 89.91 | 72.35 | 72.37 | −0.03 |
| 0.7 | 72.78 | 73.96 | −1.62 | 72.00 | 58.36 | 58.39 | −0.05 |
| 1.0 | 61.88 | 62.81 | −1.50 | 60.97 | 49.37 | 49.37 | 0.00 |
| 2.0 | 42.49 | 43.00 | −1.20 | 41.51 | 33.59 | 33.60 | −0.01 |
| 4.0 | 26.46 | 26.97 | −1.93 | 26.03 | 20.94 | 20.92 | 0.09 |
| 10.0 | 12.64 | 13.00 | −2.84 | 12.49 | 10.00 | 10.01 | 0.10 |

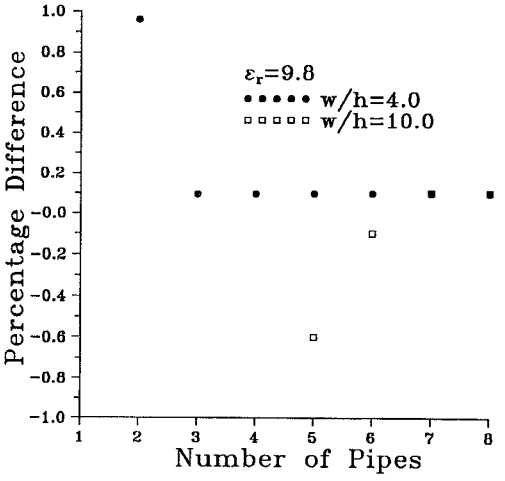


Fig. 4. Convergence of the multi-pipe model for a single microstrip line.

number of pipes is increased from 2 to 8, the percentage difference converges, by 3 pipes for $w/h = 4$ and by 7 pipes for $w/h = 10$.

*Example 2: Tightly Coupled Microstrip Lines*

Fig. 5 shows two coupled microstrips of zero thickness on a dielectric substrate above a ground plane. For various $s/h$ ratios, Table III compares our results for $\epsilon_{\text{eff, even}}$ and $\epsilon_{\text{eff, odd}}$ with those of [15]. Our results were obtained by using 5 pipes on each strip, i.e., the matrix size is 10 × 10. It is emphasized again that the pipe radii do not change in this tightly coupled situation. It is the pipe weighting coefficients, i.e., the amount of charge on each pipe, that were adjusted using the moment method to take into account the tight coupling.

*Example 3: Two Strips Between Two Ground Planes*

Fig. 6 shows two infinitely thin strips between two ground planes separated by distance $h$. The left hand strip is conductor 1, the right hand strip is conductor 2. Table

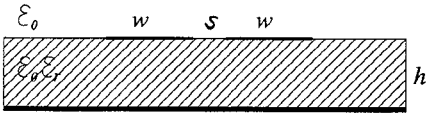


Fig. 5. Two tightly coupled microstrip lines.

IV compares our results of capacitance and inductance matrices with those of [4]. It can be seen that there are smaller relative differences between self capacitances than between mutual capacitances. In our calculations, 3 pipes were used on each strip, and the overall matrix size is 6 × 6. In [4], the matrix size was 92 × 92.

*Example 4: Three Strips in Three Different Dielectrics*

Fig. 7 shows three infinitely thin strips embedded in a three-layered dielectric between two ground planes. The left hand strip is conductor 1, the right hand strip is conductor 2, and the center strip is conductor 3. Table V compares our results of capacitance and inductance matrices with those of [4]. In our calculations, 3 pipes were used on each strip, and the overall matrix size is 9 × 9. In [4], the matrix size was 170 × 170. Again large percentage differences show up in the mutual elements with small values.

*Example 5: Six Strips on a Dielectric Substrate Above a Ground Plane*

Fig. 8 shows a six-strip transmission line geometry. The strips are numbered from left to right as 1 to 6. Table VI compares our capacitance matrix results with those of [7], [10]. We specifically checked those capacitances in which the moment method of [7] and the finite element method of [10] give significant differences. It turned out that our results consistently agree with those given by [7]. It is concluded that the HOABC-FEM (high order approximate boundary conditions in finite element method) of [10] gave errors in this example. In our calculations, 3

TABLE III
EFFECTIVE PERMITTIVITY ($\epsilon_{eff}$) FOR EVEN AND ODD MODES OF TWO TIGHTLY COUPLED MICROSTRIP LINES, $\epsilon_r = 9.8$, $w/h = 1.0$ (FIG. 5)

| | Even Mode | | | Odd Mode | | |
|---|---|---|---|---|---|---|
| $s/h$ | Our Results | Reference [15] | % Difference from [15] | Our Results | Reference [15] | % Difference from [15] |
| 0.05 | 7.047 | 7.054 | −0.099 | 5.539 | 5.542 | −0.054 |
| 0.1 | 7.064 | 7.071 | −0.099 | 5.565 | 5.571 | −0.108 |
| 0.2 | 7.093 | 7.100 | −0.099 | 5.607 | 5.615 | −0.143 |
| 0.4 | 7.132 | 7.140 | −0.112 | 5.679 | 5.687 | −0.141 |
| 0.6 | 7.154 | 7.161 | −0.097 | 5.808 | 5.817 | −0.155 |
| 1.0 | 7.125 | 7.128 | −0.042 | 5.923 | 5.931 | −0.136 |
| 2.0 | 7.011 | 7.003 | 0.114 | 6.110 | 6.111 | −0.016 |

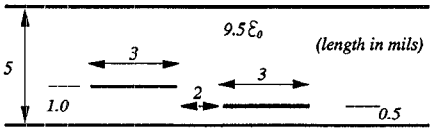


Fig. 6. Two strips between two ground planes.

TABLE IV
COMPARISON OF RESULTS FOR TWO STRIPS BETWEEN TWO GROUND PLANES (FIG. 6), (CAPACITANCE IN pF/m, INDUCTANCE IN nH/m)

| | 3 (mils) | | | 5 (mils) | | |
|---|---|---|---|---|---|---|
| $h$ | Our Results | Reference [4] | % Difference | Our Results | Reference [4] | % Difference |
| $C_{11}$ | 531.9 | 533.6 | −0.32 | 481.2 | 485.2 | −0.83 |
| $C_{12}$ | −10.096 | −9.250 | 9.15 | −1.899 | −1.798 | 5.62 |
| $C_{22}$ | 778.9 | 783.4 | −0.58 | 751.1 | 755.7 | −0.61 |
| $L_{11}$ | 198.7 | 203.3 | −2.32 | 219.8 | 224.6 | −2.18 |
| $L_{12}$ | 2.568 | 2.401 | 6.96 | 5.473 | 5.345 | 2.39 |
| $L_{22}$ | 135.7 | 139.0 | −2.43 | 140.9 | 144.2 | −2.34 |

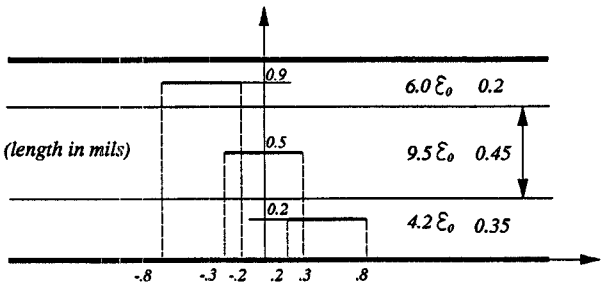


Fig. 7. Three strips in three different dielectric layers encased by two ground planes.

TABLE V
COMPARISON OF RESULTS FOR THREE STRIPS IN A THREE-LAYERED DIELECTRIC (FIG. 7), (CAPACITANCE IN pF/m, INDUCTANCE IN nH/m)

| | | $C_{ij}$ | | | $L_{ij}$ | | |
|---|---|---|---|---|---|---|---|
| $i$ | $j$ | Our Results | Reference [4] | % Difference | Our Results | Reference [4] | % Difference |
| 1 | 1 | 511.8 | 490.0 | 4.49 | 139.9 | 145.6 | −4.07 |
| 1 | 2 | −0.5916 | −0.5737 | 3.12 | 5.912 | 5.630 | 5.01 |
| 1 | 3 | −69.75 | −64.57 | 8.02 | 28.62 | 28.44 | 0.63 |
| 2 | 2 | 257.2 | 245.9 | 4.50 | 215.7 | 224.0 | −3.85 |
| 2 | 3 | −66.56 | −61.38 | 8.44 | 58.14 | 57.62 | 0.90 |
| 3 | 3 | 297.8 | 286.5 | 3.94 | 295.3 | 306.5 | −3.79 |

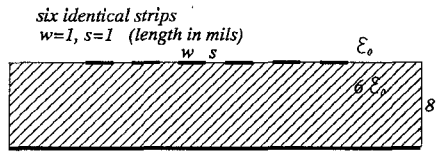


Fig. 8. Six strips on a dielectric substrate above a ground plane.

TABLE VI
COMPARISON OF RESULTS FOR A SIX-STRIP TRANSMISSION LINE STRUCTURE (FIG. 8), (CAPACITANCE IN pF/m)

| | | $C_{ij}$ | | | |
|---|---|---|---|---|---|
| $i$ | $j$ | Our Results (MoM) | Reference [7] (MoM) | % Difference from [7] | Reference [10] (FEM) |
| 1 | 1 | 67.0 | 66.8 | −0.30 | 66.7 |
| 1 | 2 | −28.0 | −27.9 | 0.36 | −29.3 |
| 1 | 3 | −5.47 | −5.49 | −0.37 | −5.65 |
| 1 | 4 | −2.05 | −2.08 | −1.50 | −1.92 |
| 1 | 5 | −0.964 | −0.999 | −3.63 | −0.792 |
| 1 | 6 | −0.647 | −0.704 | −8.81 | −0.445 |
| 2 | 5 | −1.71 | −1.73 | −1.17 | −1.55 |
| 3 | 3 | 79.6 | 79.4 | 0.25 | 81.2 |
| 3 | 6 | −2.05 | −2.08 | −1.46 | −1.92 |
| 4 | 5 | −25.7 | −25.6 | 0.39 | −26.9 |
| 6 | 2 | −0.964 | −0.999 | −3.63 | −0.792 |

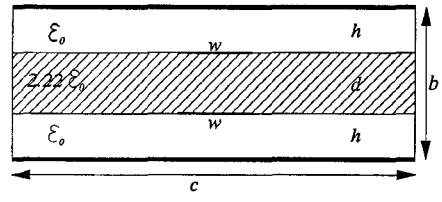


Fig. 9. Broadside coupled suspended stripline.

TABLE VII
COMPARISON OF THE EFFECTIVE DIELECTRIC CONSTANTS FOR BROADSIDE COUPLED SUSPENDED STRIPLINES, $d/b = 0.3$ (Fig. 9)

| | Odd Mode | | | Even Mode | | |
|---|---|---|---|---|---|---|
| $w/b$ | Our Results $c/w \to \infty$ | Reference [16] $c/w = 40$ | % Difference | Our Results $c/w \to \infty$ | Reference [16] $c/w = 40$ | % Difference |
| 0.1 | 1.300 | 1.303 | −0.23 | 1.713 | 1.701 | 0.71 |
| 0.2 | 1.253 | 1.255 | −0.16 | 1.744 | 1.732 | 0.69 |
| 0.4 | 1.197 | 1.198 | −0.08 | 1.779 | 1.769 | 0.56 |
| 0.8 | 1.136 | 1.138 | −0.18 | 1.811 | 1.803 | 0.44 |
| 1.5 | 1.089 | 1.088 | 0.09 | 1.842 | 1.825 | 0.93 |

pipes were used on each strip, and the overall matrix size is 18 × 18. The terms with the largest difference from [7] are again those mutual capacitances with the smallest values and thus are expected to have the largest differences.

*Example 6: Broadside Coupled Suspended Striplines*

Fig. 9 shows a broadside coupled suspended stripline. In this example, we first calculate the capacitance and inductance matrices, $[C]$ and $[L]$, and then find the eigenvalues of the matrix $[LC]$. These two eigenvalues correspond to the odd mode and even mode propagation constants, respectively. Table VII compares our results with those of [16] for the case $d/b = 0.3$. In our calculations, 5 pipes were used on each strip, and the overall matrix size is 10 × 10. In [16], there are side walls with $c/w = 40$. In our calculations we took $c/w \to \infty$. The difference in the odd mode is always less than 0.25%. This is due to the fact that the odd mode cannot see the far walls of [16] and therefore the results will compare well. For the even mode the error is still always less than 1%, but it is consistently positive, indicating that there might be some effect of the walls in the results of [16].

TABLE VIII
SPECTRAL FUNCTION $F(\gamma)$ FOR DIFFERENT SOURCE AND FIELD LOCATIONS

<table>
<tr><td>Source and field points</td><td colspan="3">$$F(\gamma)=\frac{(1-r_{si})(1-r_{fi})e^{-\gamma|y-y'|}}{1-r_{si}r_{fi}e^{-2\gamma|y-y'|}}$$</td></tr>
<tr><td>in the same dielectric layer $i$</td><td>$i=1$<br>$r_{s1}=e^{-2\gamma y'}$<br>$r_{f1}=R_1e^{-2\gamma(h_1-y)}$</td><td>$i=2$<br>$r_{s2}=R_2e^{-2\gamma(y'-h_1)}$<br>$r_{f2}=R_3e^{-2\gamma(h_1+h_2-y)}$</td><td>$i=3$<br>$r_{s3}=R_4e^{-2\gamma(y'-h_1-h_2)}$<br>$r_{f1}=e^{-2\gamma(h_1+h_2+h_3-y)}$</td></tr>
<tr><td>Source and field points in adjacent</td><td colspan="3">$$F(\gamma)=\frac{(1-r_{si})(1+r_{ij})(1-r_{fj})e^{-2\gamma|y_{ij}-y'|}}{\left(1+r_{fj}r_{ij}e^{-2\gamma|y-y_{ij}|}\right)-r_{si}e^{-2\gamma|y_{ij}-y'|}\left(r_{ij}+r_{fj}e^{-2\gamma|y-y_{ij}|}\right)}$$</td></tr>
<tr><td>dielectric layers $i$ and $j$</td><td colspan="2">$i=1 \quad j=2$<br>$r_{s1}=e^{-2\gamma y'}$<br>$r_{f1}=R_3e^{-2\gamma(h_1+h_2-y)}$ , $y_{12}=h_1$</td><td colspan="1">$i=2 \quad j=3$<br>$r_{s2}=R_2e^{-2\gamma(y'-h_1)}$<br>$r_{f3}=e^{-2\gamma(h_1+h_2+h_3-y)}$ , $y_{23}=h_1+h_2$</td></tr>
<tr><td>Source and field points separated by a dielectric layer, i.e., $i=1$ and $j=3$</td><td colspan="3">$$F(\gamma)=\frac{(1-e^{-2\gamma y'})(1+r_{12})(1+r_{23})(1-e^{-2\gamma(h_1+h_2+h_3-y)})e^{-\gamma(y-y')}}{\left[\left(1+r_{12}r_{23}e^{-2\gamma h_2}\right)-e^{-2\gamma h_1}\left(r_{12}+r_{23}e^{-2\gamma h_2}\right)\right]+e^{-2\gamma h_3}\left[\left(r_{23}+r_{12}e^{-2\gamma h_2}\right)-e^{-2\gamma t_1}\left(r_{12}r_{23}+e^{-2\gamma h_2}\right)\right]}$$</td></tr>
<tr><td>Reflection coefficients used in $F(\gamma)$ in the three rows above</td><td colspan="3">$$R_1=\frac{\left(r_{12}+r_{23}e^{-2\gamma h_2}\right)+r_{34}e^{-2\gamma h_3}\left(r_{12}r_{23}+e^{-2\gamma h_2}\right)}{\left(1+r_{12}r_{23}e^{-2\gamma h_2}\right)+r_{34}e^{-2\gamma h_3}\left(r_{23}+r_{12}e^{-2\gamma h_2}\right)} \quad , \quad R_2=\frac{r_{21}+r_{10}e^{-2\gamma h_1}}{1+r_{21}r_{10}e^{-2\gamma h_1}}$$<br>$$R_3=\frac{r_{23}+r_{34}e^{-2\gamma h_3}}{1+r_{23}r_{34}e^{-2\gamma h_3}} \quad , \quad R_4=\frac{\left(r_{32}+r_{21}e^{-2\gamma h_2}\right)+r_{10}e^{-2\gamma h_1}\left(r_{32}r_{21}+e^{-2\gamma h_2}\right)}{\left(1+r_{32}r_{21}e^{-2\gamma h_2}\right)+r_{10}e^{-2\gamma h_1}\left(r_{21}+r_{32}e^{-2\gamma h_2}\right)}$$<br>$$r_{ij}=\frac{\varepsilon_j-\varepsilon_i}{\varepsilon_j+\varepsilon_i} \quad , \quad i,j=1,2,3.$$</td></tr>
</table>

## V. CONCLUSION

In this paper, a multipipe model is presented for calculating the capacitance and inductance matrices of multistrip transmission lines in multilayer dielectric media. The multipipe model is derived from the Gauss–Chebyshev quadrature integration. It has been shown that for solving multi-strip transmission line problems, the matrix size using the multipipe model is an order of magnitude smaller than that using pulse basis functions in the moment method [1], [4]. Isolated and tightly coupled transmission lines printed on single layer substrates or embedded in multilayer dielectrics are tested. In all the examples, our results are in good agreement with published data.

The multipipe model is not limited to electrostatic problems. It can also be used in the full wave analyses of 3-D microwave integrated circuits [14], [17]. However, the multipipe model is efficient only for solving thin conducting strip problems. For transmission line conductions of arbitrary cross section, the efficiency may deteriorate.

## APPENDIX

The spectral function $F(\gamma, y, y')$ is derived for each situation in Table VIII. Only six situations of the source

and field locations are listed in Table VIII. For the other three cases, i.e., $(i = 2, j = 1)$, $(i = 3, j = 2)$ and $(i = 3, j = 1)$, one can use the same spatial Green's functions as the cases of $(i = 1, j = 2)$, $(i = 2, j = 3)$ and $(i = 1, j = 3)$ respectively, by using reciprocity.

## Acknowledgment

The authors gratefully acknowledge the constructive comments from the anonymous reviewers.

## References

[1] A. Djordjevic, R. F. Harrington, T. K. Sarkar, and M. B. Bazdar, *Matrix Parameters of Multi-Conductor Transmission Lines: Software and User's Manual*. Norwood, MA: Artech House, 1989.

[2] P. Silvester, "TEM wave properties of microstrip transmission lines," *Proc. Inst. Elec. Eng.*, vol. 115, pp. 43–48, Jan. 1968

[3] W. T. Weeks, "Calculation of coefficients of capacitance of multiconductor transmission lines in the presence of dielectric interface," *IEEE Trans. Microwave Theory Tech.*, vol. MTT-18, pp. 35–43, Jan. 1970.

[4] C. Wei, R. F. Harrington, J. R. Mautz, and T. K. Sarkar, "Multiconductor transmission lines in multilayered media," *IEEE Trans. Microwave Theory Tech.*, vol. MTT-32, pp. 437–449, Apr. 1984.

[5] H. Sobal, "Extending IC technology to microwave equipment," *Electronics*, vol. 40, pp. 112–124, Mar. 1965.

[6] F. Medina and M. Horno, "Capacitance and inductance matrices for microstrip structures in multilayered anisotropic dielectrics," *IEEE Trans. Microwave Theory Tech.*, vol. MTT-35, pp. 1002–1008, Nov. 1987.

[7] P. H Harms, C. H. Chan, and R. Mittra, "Modeling of planar transmission line structures for digital circuit applications," *Arch. Elek. Ubertragung*, vol. 43, pp. 245–250, 1989.

[8] F. Olyslager, N. Fache, and D. De Zutter, "New fast and accurate line parameter calculation of general multiconductor transmission lines in multilayered media," *IEEE Trans. Microwave Theory Tech.*, vol. 39, pp. 901–909, June 1991.

[9] G. W. Pan, K. S. Olsen, and B. K. Gilbert, "Improved algorithmic methods for the prediction of wavefront propagation behavior in multiconductor transmission lines for high frequency digital signal processors," *IEEE Trans. Computer-Aided Design.*, vol. 8, pp. 608–621, June 1989.

[10] A. Khebir, A. B. Kouki, and R. Mittra, "Higher order asymptotic boundary condition for the finite element modeling of two-dimensional transmission line structures," *IEEE Trans. Microwave Theory Tech.*, vol. 38, pp. 1433–1437, Oct. 1990.

[11] Y. L. Chow, J. J. Yang, and G. E. Howard, "Complex images for electrostatic field computation in multilayered dielectric media," *IEEE Trans. Microwave Theory Tech.*, vol. 39, pp. 1120–1125, July 1991.

[12] K. J. Binns and P. J. Lawrenson, *Analysis and Computation of Electric and Magnetic Field Problems*. Oxford: Pergamon, 1973, pp. 179–181.

[13] H. A. Wheeler, "Transmission line conductors of various cross sections," *IEEE Trans. Microwave Theory Tech.*, vol. MTT-28, pp. 73–83, Feb. 1980.

[14] D. A. Huber, "A moment method analysis of stripline circuits through multi-pipe field modeling," M.A.Sc. thesis, University of Waterloo, Waterloo, ON, Canada, Mar. 1991.

[15] R. K. Hoffman, *Handbook of Microwave Integrated Circuits*. Norwood, MA: Artech House, 1987, pp. 142, 236–239.

[16] B. Bhat and S. K. Koul, *Stripline-Like Transmission Lines for Microwave Integrated Circuits*. New York: Wiley, 1989, pp. 115, 337.

[17] P. J. Draxler, G. E. Howard, and Y. L. Chow, "Mixed spectral/spatial domain moment method simulation of components and circuits," in *Proc. 21st European Microwave Conf.*, Stuttgart, Germany, September 9–12, 1991, pp. 1284–1289.

[18] J R. Wait, "Complex image theory—revisited," *IEEE Antennas & Propag. Magazine*, vol. 33, no. 4, pp. 27–29, Aug. 1991.

**Gregory E. Howard** (S'90–M'90), for a biography, see this issue, p. 627.

**Jian Jun Yang** (M'90), for a photograph and biography, see this issue, p. 627.

**Y. Leonard Chow** (S'60–M'65), for a photograph and biography, see this issue, p. 627.